

A Unified Motion Modeling Approach for Snake Robot's Gaits Generated With Backbone Curve Method

Wei Huang , Yongchun Fang , Senior Member, IEEE, Xian Guo , Member, IEEE, Huawang Liu , and Lixing Liu

Abstract—In this article, a unified motion modeling approach for the 3-D snake robot is proposed, which enables motion prediction of all kinds of gaits generated by the backbone curve method on the ground. More specifically, the motion of the snake robot is novelly decomposed into two components, namely, the curve component and the shift component, which are explicitly related to the backbone curve's parameters and control's input. Considering the actual behavior of snake robots, a nonslip assumption is made to facilitate the modeling approach. Based on that, the ground-contacting points of the robot's links during shift control are conveniently analyzed, which helps to determine the moving direction of the curve components. Finally, with ground contacting points and backbone curve parameters determined, the characteristics of the two components, as well as the motion model, are successfully obtained. Utilizing this modeling approach, the widely used gaits, such as sidewinding, crawler, and S-pedal, are successfully modeled and then carefully analyzed to predict the movement of the snake robot with arbitrary given control input. Three groups of experiments are conducted, with the collected results showing the satisfactory accuracy of the obtained models. Compared with existing methods, the proposed modeling approach achieves a much more precise prediction, both in the direction and magnitude of snake robot motions.

Index Terms—Biologically inspired robots, redundant robots, search and rescue robots, snake robot.

I. INTRODUCTION

SNAKE robots, which are able to form various gaits with their redundancy, have received considerable attention in

Manuscript received 4 January 2024; revised 28 March 2024; accepted 9 June 2024. Date of publication 28 June 2024; date of current version 18 September 2024. This paper was recommended for publication by Associate Editor L. Wen and Editor M. Yim upon evaluation of the reviewers' comments. This work was supported in part by the National Natural Science Foundation of China under Grant 62233011, Grant 62073176, and Grant 62073328, and in part by the Haihe Lab of ITAI under Grant 22HHXJC00003. (Corresponding author: Yongchun Fang.)

Wei Huang is with the Institute of Robotics and Automatic Information System, College of Artificial Intelligence Nankai University, Tianjin 300192, China, and also with the Haihe Lab of ITAI, Tianjin 300051, China.

Yongchun Fang, Xian Guo, Huawang Liu, and Lixing Liu are with the Institute of Robotics and Automatic Information System, College of Artificial Intelligence Nankai University, Tianjin 300192, China (e-mail: fangyc@nankai.edu.cn).

This article has supplementary downloadable material available at <https://doi.org/10.1109/TRO.2024.3420803>, provided by the authors.

Digital Object Identifier 10.1109/TRO.2024.3420803

the fields of disaster area [1], narrow terrain exploration, underground pipe inspection, and so on. Numerous gaits have been presented for different tasks, such as sidewinding gait for desert and sandy soil, helical rolling gait for pipes and trees, and so on. To achieve autonomous operation, it is necessary to model the motion of the snake robot precisely. After investigating the reported results, it is known that modeling for the motion of snake robots is usually based on specific tasks with corresponding gaits. Moreover, in order to apply these gaits, various generation methods have been employed, yet they still lack a general modeling method to efficiently describe the movements of snake robots.

A general model is of great importance because it is the basis for autonomous task performance. For instance, a 2-D snake robot has an explicit general motion model, based on which, a great number of results for autonomous behavior, such as path-following, have been presented recently. Li et al. [2] proposed an adaptive controller based on the improved Serpenoid curve to accomplish the path following. Furthermore, Cao et al. [3], [4] proposed an adaptive LOS guidance law for a snake robot moving in 3-D space, which adjusts the look-ahead distance on-line to improve the accuracy of path following. A pan-tilt compensation method, together with a path-following controller, is proposed by Liu et al. [5]. Also, they propose a reinforcement learning-based hierarchical control framework [6], enabling a snake robot with an onboard camera to realize autonomous self-localization and path following. However, the currently reported models can be hardly applied to 3-D snake robots, and the lack of a general modeling method badly limits the autonomous task performance of 3-D snake robots.

Currently, the reported results on 3-D snake robots mainly focus on designing and generating specific gaits or motions, which propose various models without satisfactory generality. For example, Burdick et al. [7] revealed the kinematics of the sidewinding motion of a hyperredundant mobile robot based on the similar motion of desert snakes. Gong et al. [8] focused on the steering capabilities of sidewinding gaits and proposed an intuitive method for turning at different rates. In [9], the stability conditions for a sidewinder on a slope are identified and a minimum aspect ratio of a stable sidewinding pattern is found. Later, the sidewinding gait is extensively investigated in [10], [11], [12], and [13], and a model is set up to generate the

desired translation/rotation by corresponding turning behaviors and stable locomotion. Another gait called helical rolling gait, which is suitable for pipes/trees climbing, is carefully studied, and an extended Kalman filter is adopted to estimate gait parameters during helical climbing [14]. Takemori et al. [15] presented an irregular helical form combined with three components, and they set up models to estimate climbing states based on ground projection, achieving compliant behaviors in specific directions. For helical rolling gait, Huang et al. [16] proposed a model-based radius estimation approach and a corresponding control strategy, which result in successful autonomous climbing for pipes/trees with changing radii. More recently, models for other tasks, such as manipulation and path-following, are also carefully studied to obtain meaningful results. For example, Elsayed et al. [17] broke up the dynamics of snake robots into two parts, namely a base part in a helical shape and a manipulator part, for which kinematic models are set up separately, so as to facilitate mobile manipulation on valves. Wang et al. [18] applied a path integral reinforcement learning (PI2) framework to crawler gaits, finally learning a model and its corresponding control strategy for path-following tasks.

Mainly, the difficulties for general motion modeling of 3-D snake robots lie in the following three aspects. First of all, since various gaits are generated by different methods, it is usually very difficult to find a unified motion model for all gaits. In general, such gaits as arc rolling, slithering, and so on, are usually created with gait equations [19], [20]. On the other hand, more complicated gaits are generated by connecting backbone curve segments with the help of optimization techniques [21], [22], [23], [24], [25], which are able to accomplish challenging tasks, such as ladder climbing [26], hoop passing [27], complicated pipe structure locomotion [28], [29], and so on. Hatton and Choset [30] designed two algorithms for gait generation, which together allow a designer to conceive a motion in terms of 3-D shapes and control it by wave functions. However, for those far more complicated gaits designed with the backbone curve method that appears in the recent articles mentioned above, it is still difficult to generate them with gait equations. Besides, some slithering gait and others are generated by the central pattern generation (CPG) method [31], [32]. Second, for a snake robot, during its movement, there are numerous contact points between the robot and the environment, which are time-varying, adding much more complexity to the modeling task. Last but not least, some uncertain factors, such as the slips during the movement due to insufficient friction, need to be carefully considered to obtain models with satisfactory accuracy. Due to these difficulties, motion modeling for 3-D snake robots remains a fairly open problem.

So far, some results for motion modeling of 3-D snake robots have been reported. Transeth et al. [33] developed a 3-D mathematical model of a snake robot based on the framework of non-smooth dynamics and convex analysis. Enner et al. [34] utilized the virtual chassis to separate the snake robot's internal shape changes from its external motions, then constructed a motion model based on the differential motion of the robot's modules between time steps. Melo [35] utilized a floating frame of

reference and ground static contact to determine the magnitude and direction of sidewinding motion, and proposed a velocity model of snake robots. However, existing methods mainly analyze the motion process of each module but do not utilize the backbone curve of gaits. Due to this reason, the motion modeling results remain complicated and only applicable for gaits generated by parameterized gait equations with relatively simple 3-D shapes. Moreover, the motion modeling results are not precise enough, especially in the direction prediction.

Although not many results have been reported in recent years, motion modeling is significant for autonomous behaviors of snake robots. Because of these difficulties in building general motion models for 3-D snake robots, recent works studying autonomous locomotion utilize some data-driving [36], [37] or control-to-action mapping [38] methods with additional controllers. Autonomous behaviors are achieved but several drawbacks are apparent: first the data-collection process can be tedious and repetitive. Furthermore, the model acquired is highly sensitive to variations in gait shape and the physical conditions of the environment. Its limited interpretability poses challenges for fine-tuning or modification. Last, these presented methods are mainly applied to gaits with relatively simple shapes, the autonomous locomotion of complicated 3-D gait remains undeveloped.

Considering the current research status, this article studies the modeling of the on-ground motion of snake robots and proposes a unified motion modeling approach for gaits generated with the backbone curve method. Compared with existing results, the contributions and advantages of this article lie in the following aspects.

- 1) Instead of purely focusing on analyzing the motion process of each module, our method also utilizes the backbone curve of gaits, so as to decompose the motion of the snake robot into movements of the backbone curve and movements of the robot along the backbone curve. Therefore, the proposed approach is generally applicable to complicated gaits generated with the backbone curve method and results in explicit motion models.
- 2) With the help of the proposed modeling approach, the motion models for widely used gaits generated by the backbone curve method, such as S-pedal, sidewinding, and crawler gaits, are successfully set up to fulfill autonomous control for snake robots.
- 3) Several sets of experiments are conducted, with the collected results clearly validating the satisfactory accuracy of the obtained motion models. Compared with existing methods, the proposed modeling approach achieves much more precise prediction, both in the direction and magnitude of robot motion.

The rest of this article is organized as follows. The background of the backbone curve method, together with shift control, is provided in Section II. Then, a unified modeling approach is designed in Section III, with S-pedal gait as an illustrative example. To prove the generality of the proposed modeling approach, it is further utilized to model some other gaits in Section IV. After that, some experiments are conducted, and the obtained results

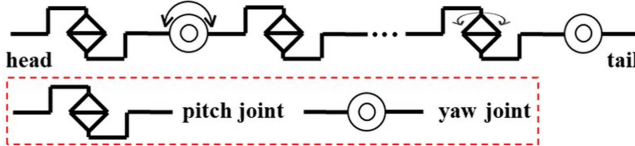


Fig. 1. Joints layout of a 3-D snake robot.

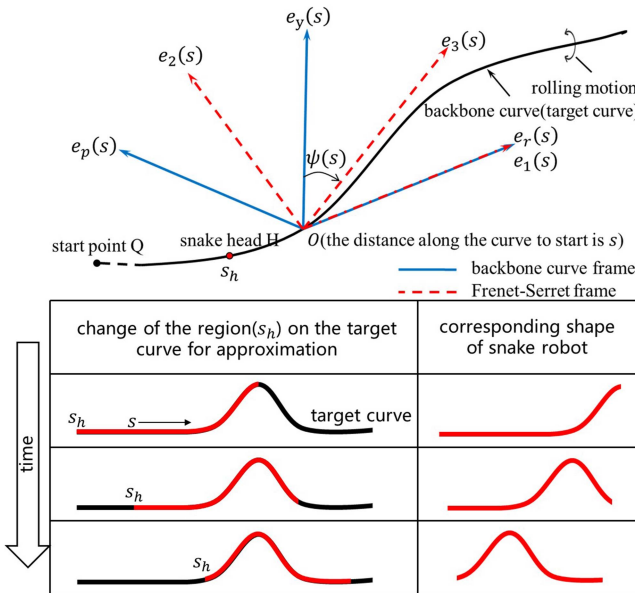


Fig. 2. Upper side: Frenet–Serret frame and backbone curve frame. Lower side: Demonstration of shift control.

are provided in Section V, as well as performance discussions. Finally, Section VI concludes this article.

II. BACKGROUND OF BACKBONE CURVE METHOD

The snake robot discussed in this article is composed of serially connected links via alternating pitch and yaw joints, whose joint layout is shown in Fig. 1.

The backbone curve method, which considers the target shape of the robot as a spatial curve, is suitable for the analysis of the target shape with known curvature κ and torsion τ . According to [21], [22], [23], and [24], joint angles are calculated based on the target curve

$$\theta_i = \begin{cases} \int_{s_h+(i-1)l}^{s_h+(i+1)l} -\kappa(s) \sin \psi(s) ds, & i \text{ is odd} \\ \int_{s_h+(i-1)l}^{s_h+(i+1)l} \kappa(s) \cos \psi(s) ds, & i \text{ is even} \end{cases} \quad (1)$$

where i is the joint number and l denotes the length of the link. To focus on the modeling approach, only major factors are considered during the modeling process, and all the links of the snake robot are assumed of the same length. To better explain the other variables in (1), including $\kappa(s)$, $\psi(s)$, s_h , and so on, two key frames, namely, the Frenet–Serret frame and the backbone curve frame, are illustrated in the upper plot of Fig. 2, so as to formulate Yamada's motion generating method. As shown in the

figure, $e_1(s)$, $e_2(s)$, and $e_3(s)$ are unit orthonormal vectors intersecting at the point O , forming the basis of *Frenet–Serret frame* drawn with blue lines, with s denoting the distance between O and the starting point Q of the curve, where $e_1(s)$ and $e_2(s)$ denote the tangent vector and the normal vector of the curve at the point O , while $e_3(s)$ is fixed according to the right-hand rule. The other frame, known as the *backbone curve frame*, is drawn with red dash lines, where the axis $e_r(s)$ coincides with the axis $e_1(s)$ of the Frenet–Serret frame, while $e_p(s)$ and $e_y(s)$ are set along the snake robot joints' pitch axis and yaw axis at the point O , respectively.

As shown in the upper plot of Fig. 2, the rotation around the axis $e_1(s)$ (or $e_r(s)$) between the Frenet–Serret frame and the backbone curve frame, namely, twist angle $\psi(s)$, can be calculated as

$$\psi(s) = \int_0^s \tau(\hat{s}) d\hat{s} + \psi(0) \quad (2)$$

where $\tau(s)$ is the curve's torsion in the Frenet–Serret frame, and $\psi(0)$ denotes the initial condition which is directly related to the rolling of the snake robot and thus called rolling angle as well.

As shown in the lower part of Fig. 2, s_h is the distance between the snake robot's head point H and the curve start point Q on the target curve. By changing s_h , *shift control* is employed. That is, when s_h changes with time, the snake robot will approximate the shape of the given target form.

Usually, it is difficult to find a unified curvature κ and torsion τ when representing a complicated target form for snake robots. Instead, separating the target curve into several simple curve segments is a feasible solution. Takemori et al. [24] provided a method in which the target form was implemented by connecting curve segments, including the straight line, the circular arc, and the helix. In general, a complex target form can be constructed by carefully selecting the needed curve segments and then connecting them in a specific order. Besides, the joint angle can be calculated using the backbone curve method since the curvature and torsion are available.

The calculation process for joint angles is somewhat similar to the backbone curve method mentioned before, with the main difference being that the connection part of curve segments should be reconsidered. Because the Frenet–Serret frame becomes discontinuous at the connection part, a correction of representation is needed. As shown in Fig. 3, segment j ($j \in \mathbb{Z}$) is the j th segment counting from the start point of the target shape, and $s = s_j$ is the connection point of segment j and $j + 1$. Segments j and $j + 1$ are in contact with each other at $s = s_j$. s_{j-} and s_{j+} denote points with an infinitesimal distance before and after connection point j . Without loss of generality, the curvature and torsion, as well as the Frenet–Serret frame at s_j , are represented by those at s_{j-} .

To represent the curvature and torsion of the target form, the curvature and torsion of segment j are denoted as $\kappa_j(s)$ and $\tau_j(s)$, while the point $s = 0$ in $\kappa_j(s)$ and $\tau_j(s)$ is the starting point of segment j . The curvature $\kappa(s)$ and torsion $\tau(s)$ of the

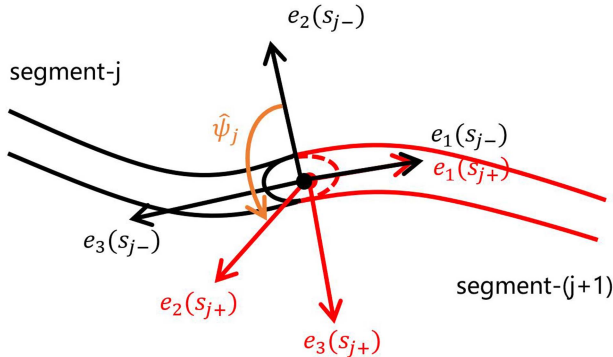


Fig. 3. Connecting point of segment j and $j + 1$.

target form can be obtained as

$$\begin{aligned}\kappa(s) &= \kappa_j(s - s_{j-1}) \quad (s_{j-1} < s \leq s_j) \\ \tau(s) &= \tau_j(s - s_{j-1}) \quad (s_{j-1} < s \leq s_j).\end{aligned}\quad (3)$$

In Fig. 3, the twist angle $\hat{\psi}_j$ needs to be designed for each segment, which is defined as the angle between $e_2(s_{j-})$ and $e_2(s_{j+})$ around $e_1(s_{j-})$. To consider this specified twist angle in the backbone curve method, (2) is changed to

$$\psi(s) = \int_0^s \tau(\hat{s})d\hat{s} + \psi(0) + \sum_j \hat{\psi}_j u(s - s_j) \quad (4)$$

where $u(s)$ is the step function

$$u(s) = \begin{cases} 0 & (s < 0) \\ 1 & (s \geq 0). \end{cases} \quad (5)$$

The variation of $\hat{\psi}_j$ leads to a rolling action at the corresponding connection part of the target form. Then the joint angles of snake robots can be obtained by utilizing (1), (3), and (4). In order to design a gait, the corresponding target shape needs to be determined in advance, which requires the determination of the shape and twist angle $\hat{\psi}_j$ of each segment, as well as the total number of segments.

III. A UNIFIED MOTION MODELING APPROACH FOR GAITS GENERATED WITH BACKBONE CURVE METHOD

A. Modeling Procedure Overview

The proposed approach provides a unified motion modeling process for the snake robot's on-ground gaits generated with the backbone curve method. Specifically, as shown in Fig. 4, the movement of the snake robot's gaits is decomposed into two parts, namely, the motion of the backbone curve d_{curve} and the motion of the snake robot along backbone curve d_{shift} , which have explicit relations with backbone curve parameters and shift control's input Δs_h . The decomposition is achieved by utilizing a novel recognition that considers the target curve as a real entity with the ability to move. To better take account of the main factors during the modeling process, a nonslip assumption is made. Based on this assumption, the ground-contacting statements of the snake robot's links during shift control are analyzed, which helps to determine the direction ϕ of d_{curve} . Finally, with ground

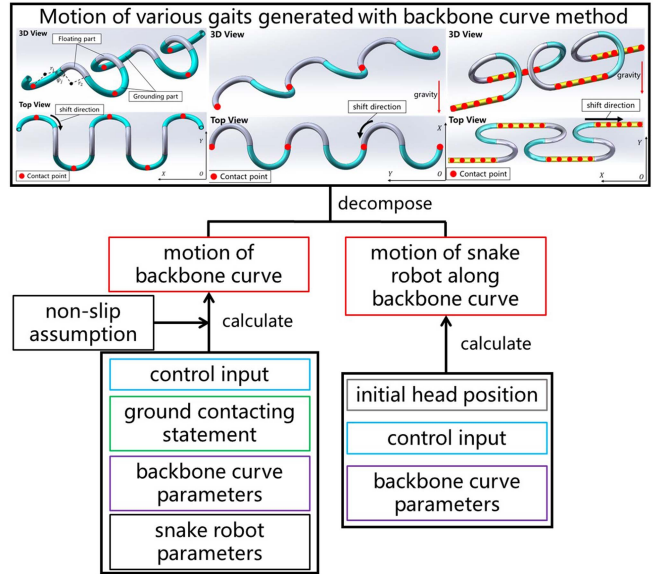


Fig. 4. Demonstration of procedure of proposed motion modeling approach.

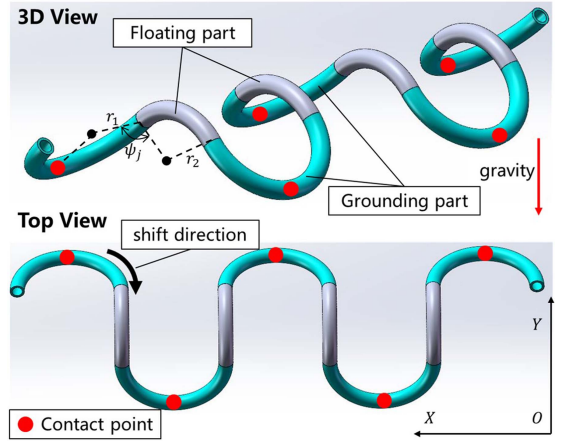


Fig. 5. Demonstration of S-pedal gait's target curve, where the cyan parts are contacting the ground and the gray parts are in the air. The ground-contacting point is marked with red circles.

contacting statement, as well as the control input and backbone curve parameters, the motions d_{curve} and d_{shift} can be calculated, which then helps to set up the motion model.

To provide a concrete demonstration of the modeling approach, a gait called S-pedal shown in Fig. 5, which appears in reported results [26] and is suitable for ground and uneven terrain such as ruins and debris field, is used as an illustrative example here.

B. Modeling of S-Pedal Gait

1) *Gait Design and Its Backbone Curve Parameters:* The S-pedal gait is developed to achieve stable movements on the ground with the leg part formed by several links. As shown in Fig. 5, the target shape consists of arcs, the minimum segments unit includes two grounding parts and two floating parts, where the tops of cyan circular parts are contacting ground and gray parts are in the air. The grounding parts serve as legs and provide

TABLE I
PARAMETERS OF GAITS

seg no. j	part	shape	parameter
$4m + 1$	ground part	circular arc	$(r_1, \pi, \hat{\psi}_j = -\pi/2)$
$4m + 2$	floating part	circular arc	$(r_2, \beta, \hat{\psi}_j = \pi/2)$
$4m + 3$	ground part	circular arc	$(r_1, \pi, \hat{\psi}_j = \pi/2)$
$4m + 4$	floating part	circular arc	$(r_2, \beta, \hat{\psi}_j = -\pi/2)$

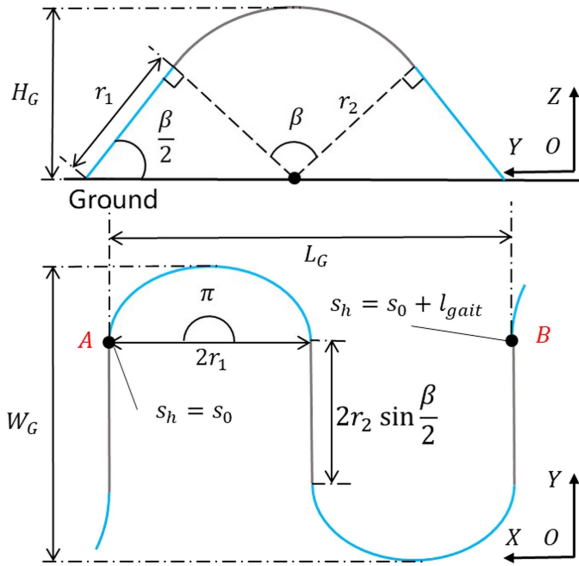


Fig. 6. Projections of S-pedal gait curve on YOZ and XOY planes with key parameters, where the cyan parts are contacting ground and gray parts are in the air.

friction force for movements. The gait is designed and realized by connecting backbone curve segments [24], which has been briefly introduced in Section II. Without loss of generality, we assume the direction of shift control with the black solid arrow in Fig. 5 to facilitate subsequent analysis.

The parameters for the segments to form S-pedal gait are shown in Table I. Specifically, the gait unit consists of four segments, with each segment presenting three key parameters, namely radius, arc angle, and twist angle. The twist angle indicates the direction difference of radius at connecting points (see Fig. 5), which is set as $\frac{\pi}{2}$ for this gait.

As introduced in the modeling procedure, we first figure out the gait's backbone curve parameters by utilizing the parameters of segments.

Fig. 6 illustrates the projections of the S-pedal gait curve on YOZ and XOY planes, where the ground-contacting part and the floating part are, respectively, drawn in cyan and gray. r_1, r_2 denotes the radius of grounding arc and floating arc in respect, and their angles are listed in Table I, $\frac{\beta}{2}$ represents the angle between ground and grounding arc. For stability and convention, the center of the floating arc is set on the ground, which is the black dot in Fig. 6. With r_1, r_2 manually settled, β can be calculated as

$$\beta = 2 \arctan \frac{r_2}{r_1}. \quad (6)$$

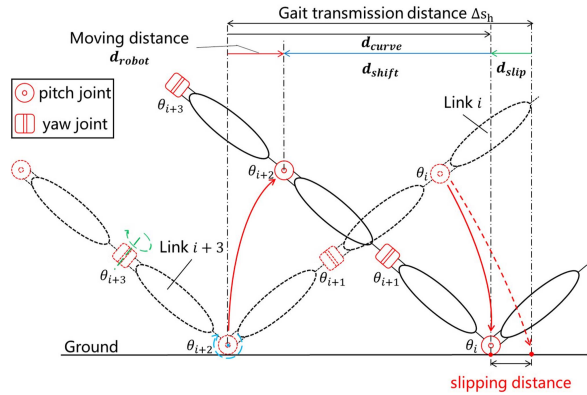


Fig. 7. Simplified general process of contact part transmission in shift control with slips, robot at time t is represented by dash lines, after a short time Δt , it reaches the new position represented with solid lines. The corresponding body shape, as well as the contact point, is transferred from joint $i + 2$ to joint i .

Then the parameters of S-pedal gait's backbone curve are calculated as

$$\begin{cases} L_G &= 4r_1 \\ W_G &= 2r_1 \cos \beta + 2r_2 \sin \frac{\beta}{2} \\ H_G &= r_2 \\ l_{gait} &= 2r_1\pi + 2r_2\beta \end{cases} \quad (7)$$

where l_{gait} denotes the least periodic length of the 3-D curve, and L_G denotes the length along the X -direction of a gait cycle. The width W_G and height H_G determine the situation that the S-pedal gait is capable of passing through.

2) *Motion Modeling of Gait in Shift Control. Assumption:* The ground-contacting points do not slip during locomotion, which is reasonable for situations with normal friction coefficients.

We illustrate the kernel of the proposed modeling approach with Fig. 7, which is the general process of contact part transmission in shift control with slips. Please note that it is simplified to a 2-D case for a clear view. The assumption will be utilized later as a key condition.

For a snake robot, when applying shift control, the movements are achieved by periodically transmitting the shape from its head to its tail. Therefore, the contact points are also transmitted between links, as shown in Fig. 7, with the red parts being the pitch and yaw joints, while the ellipses represent the links. The robot at time t is represented with dash lines, after a short time Δt , it moves to the new position represented by solid lines. The body shape is passed forward from joint $i + 2$ to joint i , causing joint i (also the robot) to move forward. Noting that for shift control, the gait transmission distance Δs_h is regarded as the control input, the corresponding moving distance d needs to be mathematically related to the control input and other involved parameters so as to build the motion model.

Noticing that Fig. 7 is only a simplified process for illustration, it is difficult to fully analyze the actual contact point transmission because of the following.

- 1) Unlike Fig. 7, for a gait with a relatively complicated shape, the pitch and yaw joints all take part in the transmission and form a 3-D shape with joint angles, which makes

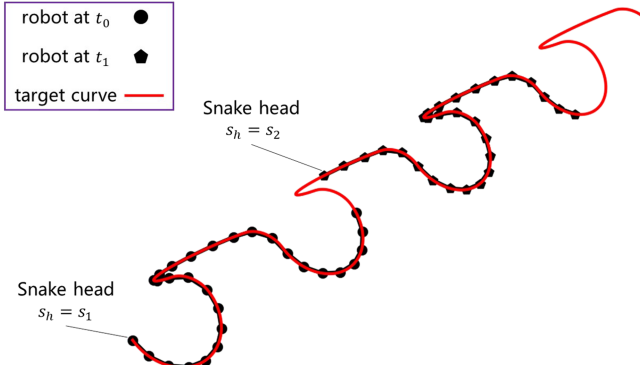


Fig. 8. Side view of S-pedal gait with shift control, the snake robot travels along this target curve as a train travels along the railway.

it difficult to analyze the change of ground-contacting state.

- 2) Due to the discontinuous structure of the snake robot, during the transmission shown in Fig. 7, joints angle Θ , as well as body shape, changes all the time, leading to tedious repeating modeling tasks.

In order to address these difficulties, a convenient analysis method for the motion model is presented. It avoids tedious modeling based on the robot's shape and joint angles, which are time-variant. Instead, the proposed modeling method focuses on the overall 3-D shape of the target curve, which is fixed once the gait parameters are determined.

Fig. 8 shows the shift control motion of S-pedal gait in a 3-D case. The red line denotes the target curve, it repeats until the gait is further modified. In the curve, the circles represent the locations of the snake robot with its head position at $s_h = s_1$, while the pentagons are for the robot with the head position of $s_h = s_2$. As we mentioned earlier, the essence of shift control is to make the snake robot travel along the given target curve, similar to how a train travels along the railway. Noting that each part of the robot will contact the ground and there is no slip as the assumption states, the target curve is regarded as a real entity with moving ability, and the movement of the snake robot is then decomposed into two parts, namely the movement of the target curve in the world coordinates and the movement of the snake robot along the target curve. Denote the motion of the target curve as d_{curve} , and the motion of the robot along the target curve as d_{shift} , then the actual motion of the snake robot, denoted as d_{robot} , can be calculated as:

$$d_{\text{robot}} = d_{\text{curve}} + d_{\text{shift}}. \quad (8)$$

As shown in Fig. 7, the magnitude of d_{curve} should be

$$|d_{\text{curve}}| = \Delta s_h + |d_{\text{slip}}| \quad (9)$$

where d_{curve} is the displacement of the target curve. Without slips, its magnitude equals the gait transmission length Δs_h , while its direction is determined by the ground-contacting status. Therefore, the nonslip condition then guarantees $|d_{\text{slip}}| = 0$ to obtain a feasible calculation of d_{curve} .

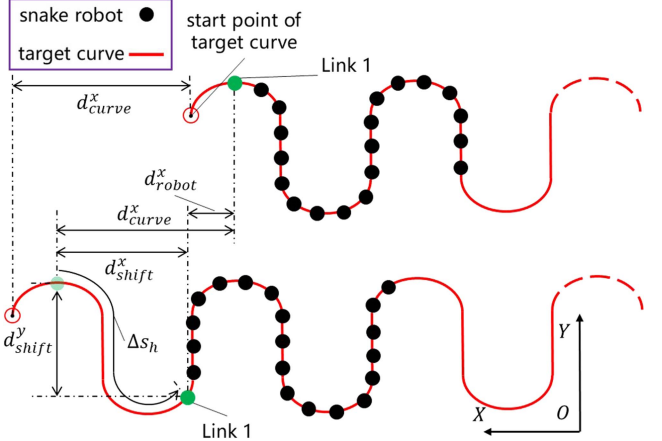


Fig. 9. Top view of the movements of the S-pedal target curve and snake robot for shift control.

The direction of d_{curve} and d_{shift} still need to be determined. Apparently, d_{shift} is in the direction tangent to the corresponding target shape curve. Further, the direction of d_{curve} can be figured out by carefully investigating the ground-contacting statement of the snake robot's links during movements. As shown in Fig. 7, the movement of the target curve is caused by the ground-contacting part transmitting between links. For the S-pedal gait's projection on the XOY plane in Fig. 6, the contacting point is at the top of the grounding arcs, which are located on both sides of the gait. Based on the assumption of nonslip, it is obvious that the direction of d_{curve} is along the X-direction, implying that d_{curve}^y for S-pedal gait is 0. It should be pointed out that, this is the most straightforward case for direction analysis, other gaits such as sidewinding, need further calculations, which will be introduced in the next section. As shown in Fig. 9, with an arbitrary Δs_h , it is able to separate (8) into X- and Y-directions as

$$\begin{cases} d_{\text{robot}}^x = d_{\text{curve}}^x - d_{\text{shift}}^x \\ d_{\text{robot}}^y = d_{\text{curve}}^y - d_{\text{shift}}^y = -d_{\text{shift}}^y \end{cases} \quad (10)$$

Considering the nonslip assumption, the moving distance of the target curve is the curve length that the snake robot travels along this target curve, in the sense that

$$d_{\text{curve}}^x = \Delta s_h \quad (11)$$

where Δs_h is the gait transmission distance, also regarded as the shift control input. d_{shift} is caused by the shift control indicating that the snake robot moves along the target curve when s_h changes smoothly. From Fig. 9, the variable d_{shift} of the gait is calculated as

$$\begin{cases} d_{\text{shift}}^x = \frac{\int_{s_{h0}}^{s_{h0} + \Delta s_h} ds \cdot e_x}{|e_x|} \\ d_{\text{shift}}^y = \frac{\int_{s_{h0}}^{s_{h0} + \Delta s_h} ds \cdot e_y}{|e_y|} \end{cases} \quad (12)$$

where e_x, e_y are vector units along X- and Y-axes, respectively. While s_{h0} is the original position for the head of the robot on the target curve, and ds is an infinitely short vector on the target curve. Equation (12) reveals that d_{shift} is the projection of its

corresponding target curve with control input Δs_h . Combining (10)–(12), the moving distance of the robot for S-pedal gait with shift control input Δs_h is obtained as

$$\begin{cases} d_{\text{robot}}^x = \Delta s_h - \frac{\int_{s_{h0}}^{s_{h0} + \Delta s_h} ds \cdot e_x}{|e_x|} \\ d_{\text{robot}}^y = -\frac{\int_{s_{h0}}^{s_{h0} + \Delta s_h} ds \cdot e_y}{|e_y|}. \end{cases} \quad (13)$$

Unfortunately, in (13), the direction of the signal ds is time-varying, making d_{robot}^x and d_{robot}^y as nonlinear functions of the input Δs_h , as well as affected by the initial position of the robot's head s_{h0} . To obtain an analytical expression for d_{robot} , the periodicity of the target curve with shape parameters in (7) is utilized to facilitate analysis.

The gait transmission distance Δs_h is set as the length of one gait unit l_{gait} in (7), such as the length from point A to point B along the target curve in Fig. 6. For this case, the corresponding signals \hat{d}_{shift} and \hat{d}_{curve} in Fig. 6 can be determined as

$$\begin{cases} \hat{d}_{\text{curve}}^x = l_{\text{gait}} = 2r_1\pi + 2r_2\beta \\ \hat{d}_{\text{shift}}^x = L_G = 4r_1 \\ \hat{d}_{\text{shift}}^y = 0. \end{cases} \quad (14)$$

Substituting (14) into (10), the periodic motion model for the S-pedal gait is finally obtained

$$\begin{cases} \hat{d}_{\text{robot}}^x = 2r_1\pi + 2r_2\beta - 4r_1 \\ \hat{d}_{\text{robot}}^y = 0 \end{cases} \quad (15)$$

where \hat{d}_{robot}^x and \hat{d}_{robot}^y represent the movements of the robot when Δs_h is set to one gait unit's length l_{gait} .

It should be noted that the proposed modeling approach is also applicable to other gaits designed by connecting backbone curve segments. In general situations, the signal d_{curve} is represented as

$$\begin{cases} |d_{\text{curve}}| = \Delta s_h \\ \phi = \frac{d_{\text{curve}} \cdot e_x}{|d_{\text{curve}}|}. \end{cases} \quad (16)$$

In (16), the signal ϕ denotes the angle between d_{curve} and the positive direction of X axis. For S-pedal gait discussed in this section, $\phi = 0$, since its d_{curve} is always along X -axis. The calculation of d_{shift} has been provided in (12), combining (8), (12), and (16), the motion modeling of gait generated with the backbone curve method is eventually completed.

For other gaits, such as sidewinding gait, although the directions of d_{curve} and d_{shift} are different from those of S-pedal, the model (8), (12), and (16) are still applicable. In the next section, the modeling approach will be employed on widely used gaits developed by backbone curve segments.

It should be noted that although the proposed motion modeling method is based on backbone curves, its potential applications are not limited to gaits generated with backbone curves. By utilizing gait-converting methods [24], [30], [39], gaits generated by other methods can be generated in the form of backbone curves and utilize the proposed approach.

C. Modeling Accuracy Analysis

The motion models built with the proposed approach unavoidably contain accumulation error over a long period of movement.

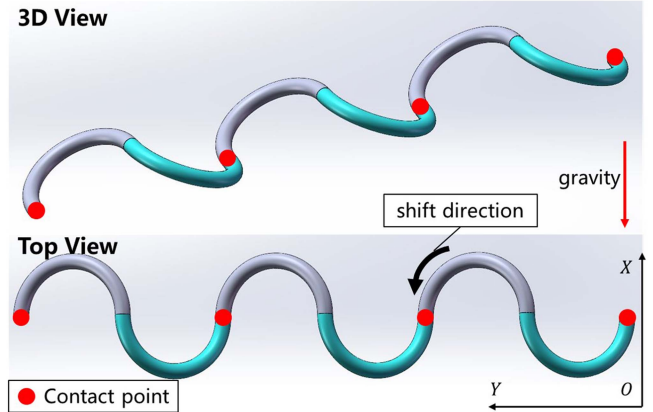


Fig. 10. Demonstration of sidewinding gait's target curve, where every other connecting point marked in red is contacting the ground.

Here, a discussion about the modeling error is provided, as shown in (16), the magnitude of d_{curve} is calculated as the length of the corresponding continuous target shape, yet the snake robot has a discrete structure with connected links. Hence, the error for the presented models during movements is indeed the error of curve approximation, and it accumulates proportionally when fitting more target curves in the situation of moving for a longer period. The curve approximation error has been carefully investigated in articles about the backbone curve method [40]. It proves that first of all, when compared with configurations such as using the universal joint or including roll axis joint, the joint configuration used in this article achieves the highest accuracy. Second, the approximation error is proportional to the -2 power of the number of links per length. It will be verified in the subsequent experiments that the error is too small to affect the effectiveness of the proposed modeling approach.

IV. APPLICATION OF THE MODELING APPROACH TO OTHER GAITS

To demonstrate the generality of the proposed modeling approach, two widely used gaits generated with backbone curve segments, namely sidewinding [19], [25], [26], [41] and crawler [24], [26], [27], are utilized as illustrative examples to set up corresponding motion models. Sidewinding gait is developed based on the movements of biological snakes on sandy terrain, while crawler gait is suitable for uneven terrain such as ruins and debris fields.

A. Sidewinding Gait Modeling

The sidewinding gait developed from backbone curve segments has the target curve shown in Fig. 10. A certain shift direction is assumed for the convenience of analysis. The minimum gait unit consists of two half-circle arcs with parameters displayed in Table II. Compared with Table I, there is no "part" column in this table since each arc is in contact with the ground.

To model the sidewinding gait, the first step is to figure out the curve parameters of the gait. Fig. 11 plots the projections of sidewinding gait's target curve on XOZ and XOY planes, whose

TABLE II
PARAMETERS OF GAITS

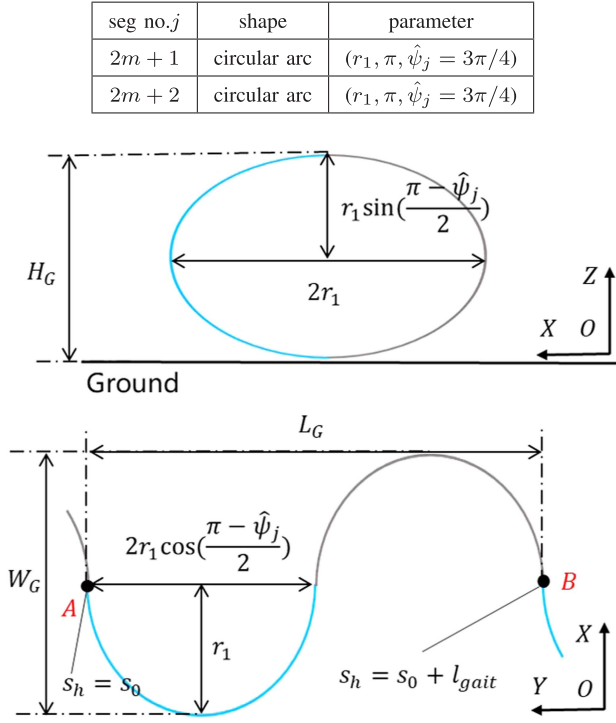


Fig. 11. Projections of sidewinding gait curve on XOZ and XOY planes with key parameters.

minimum gait cycle consists of two half circular arcs with the same radius r_1 , the signal $\hat{\psi}_j$ denotes the twist angle at the connecting point between adjacent arcs. Based on the geometric relationship shown in Fig. 11, the curve parameters are obtained as

$$\begin{cases} L_G = 4r_1 \cos \frac{\pi - \hat{\psi}_j}{2} \\ W_G = 2r_1 \\ H_G = 2r_1 \sin \frac{\pi - \hat{\psi}_j}{2} \\ l_{gait} = 2\pi r_1. \end{cases} \quad (17)$$

Subsequently, we adopt (8), (16), and (12) to complete the modeling process. Nevertheless, the angle ϕ in (16), representing the moving direction of the target curve, is no longer along X -axis, which thus involves additional analysis.

As shown in Fig. 10, the contact points of the sidewinding gait are every other connecting point of adjacent arcs. If the snake robot is perfectly smooth and continuous as the target curve, the direction of d_{curve} , with the presumed shift direction, should be along the tangent of the point, which is along X -axis. Unfortunately, unlike S-pedal gait with ground-contacting points located on both sides and as shown in Fig. 1, the snake robot has a discrete structure, which then leads to a deviation. The process of transmitting contacting points of sidewinding gait is demonstrated in Fig. 12 (the top view of gait is amplified), where the circles indicate the robot's joints with the currently contacting ground one marked in red. In the figure, the solid cyan and gray curves are the projections of two half-circular segments on the XOY plane, whereas the dashed gray curve is

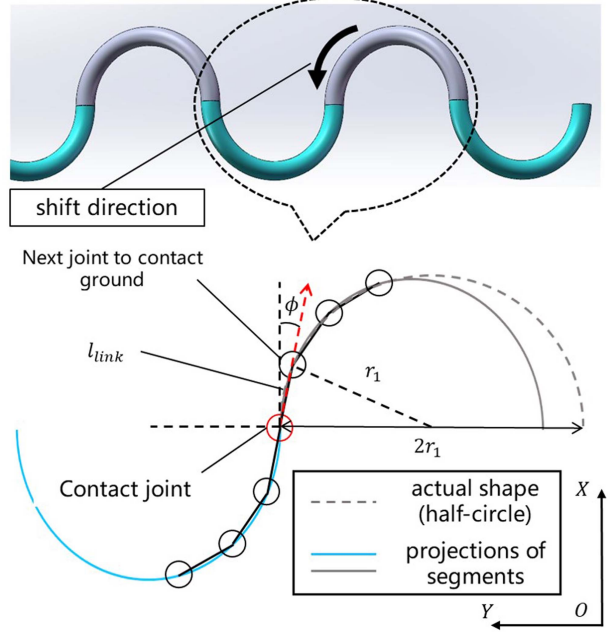


Fig. 12. Amplified demonstration of transmitting the contacting point of sidewinding gait, the circles indicate the snake robot's joints and the currently contacting ground one is marked in red. The solid cyan and gray curves are the projections of two half-circular segments on the XOY plane, whereas the dashed gray curve is the actual shape (half-circle). The direction of d_{curve} is indicated by the red dashed arrow.

their actual shape. The direction of d_{curve} , with a deviation of ϕ from X -axis, is represented by the red dashed arrow. Denote the length between joints as l_{link} , which is a fixed parameter for the studied snake robot, the direction of d_{curve} is obtained as

$$\phi = \frac{l_{link}}{2r_1}. \quad (18)$$

Because the grounding joint is on the projected plane, the projection almost coincides with the actual shape curve nearby. Noting that the signal l_{link} is relatively small, in (18), the arc length is replaced with l_{link} and it is considered on the half circle.

After the direction of d_{curve} is determined, (8) can be applied. d_{curve} and d_{shift} are also separated into scalars in X - and Y -axes, respectively. Notice that d_{curve} is no longer along X -axis, implying $d_y^{curve} \neq 0$. A general demonstration of (8) for sidewinding gait is shown in Fig. 13, which yields a specific form of (8)

$$\begin{cases} d_x^{robot} = d_x^{curve} - d_x^{shift} \\ d_y^{robot} = d_y^{curve} - d_y^{shift} \end{cases} \quad (19)$$

where d_{shift} is obtained from (12). In Fig. 12, the direction of d_{curve} stays invariant until the robot moves, whereas d_{shift} has a time-varying direction according to (12), because it is tangential to the target curve. Substituting (16), (12), and (18) into (19), the motion model of the sidewinding gait with shift control input Δs_h is built as

$$\begin{cases} d_x^{robot} = \Delta s_h \cos \phi - \frac{\int_{s_{h0}}^{s_{h0} + \Delta s_h} ds \cdot e_x}{|e_x|} \\ d_y^{robot} = \Delta s_h \sin \phi - \frac{\int_{s_{h0}}^{s_{h0} + \Delta s_h} ds \cdot e_y}{|e_y|} \\ \phi = \frac{l_{link}}{2r_1}. \end{cases} \quad (20)$$

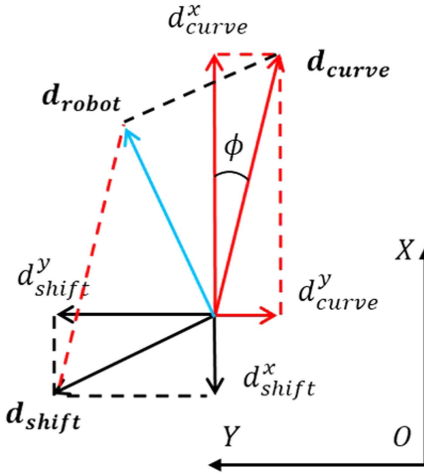


Fig. 13. Decompose d_{curve} and d_{shift} into two directions for sidewinding gait.

Based on (20), the movements of sidewinding gait can be modeled with any control input Δs_h . It should be noted that ϕ is only the direction angle of d_{curve} , the direction angle of the robot's motion is calculated by the d_{robot}^x and d_{robot}^y . In order to remove the time-variant direction of d_{curve} , we also provide the periodic model with the control input Δs_h set to one gait unit l_{gait} , which is calculated in (17).

The curve length between point A and point B in Fig. 11 is l_{gait} , when the control input Δs_h is set to l_{gait} , the corresponding \hat{d}_{curve} and \hat{d}_{shift} can be obtained in Fig. 11 as

$$\begin{cases} \hat{d}_{\text{curve}}^x = l_{\text{gait}} \cdot \cos \phi = 2\pi r_1 \cos \phi \\ \hat{d}_{\text{curve}}^y = l_{\text{gait}} \cdot \sin \phi = 2\pi r_1 \sin \phi \\ \hat{d}_{\text{shift}}^x = 0 \\ \hat{d}_{\text{shift}}^y = L_G = 4r_1 \cos \frac{\pi - \hat{\psi}_j}{2} \\ \phi = \frac{l_{\text{link}}}{2r_1}. \end{cases} \quad (21)$$

Substituting (21) in (19), the periodic motion model of the sidewinding gait is obtained

$$\begin{cases} \hat{d}_{\text{robot}}^x = 2\pi r_1 \cos \phi \\ \hat{d}_{\text{robot}}^y = 2\pi r_1 \sin \phi - 4r_1 \cos \frac{\pi - \hat{\psi}_j}{2} \\ \phi = \frac{l_{\text{link}}}{2r_1}. \end{cases} \quad (22)$$

Further, the sidewinding model will also be verified with the experiment in Section V.

Remark: The sidewinding gait model built in this section is different from those generated by the gait equation method presented in [10] and [19], although both can achieve side moving, with the main difference in shape and control method, thus requiring a different modeling approach.

B. Modeling Crawler Gait

The crawler gait presented in [24] has the target curve shown in Fig. 14. As similarly done for the sidewinding gait, a shift direction is assumed for the convenience of analysis. The minimum gait unit consists of 4 half-circle arcs and 2 lines with parameters displayed in Table III.

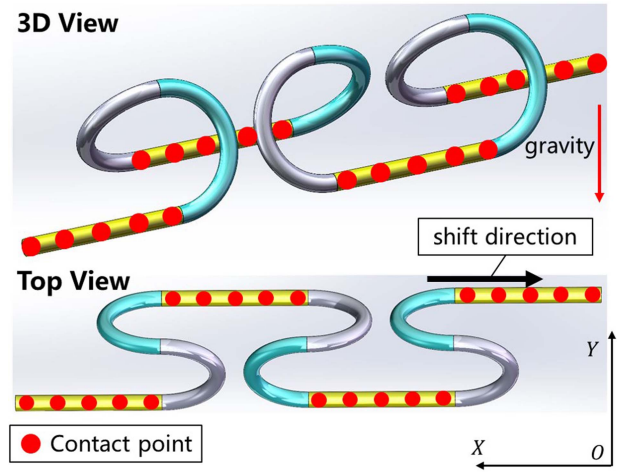


Fig. 14. Demonstration of crawler gait's target curve, where the straight line parts are contacting the ground.

TABLE III
PARAMETERS OF GAITS

seg no. j	shape	parameter
6m + 1	straight line	$(2r_1 + d, \hat{\psi}_j = 0)$
6m + 2	circular arc	$(r_1, \pi, \hat{\psi}_j = \alpha)$
6m + 3	circular arc	$(r_1, \pi, \hat{\psi}_j = 0)$
6m + 4	straight line	$(2r_1 + d, \hat{\psi}_j = 0)$
6m + 5	circular arc	$(r_1, \pi, \hat{\psi}_j = -\alpha)$
6m + 6	circular arc	$(r_1, \pi, \hat{\psi}_j = 0)$

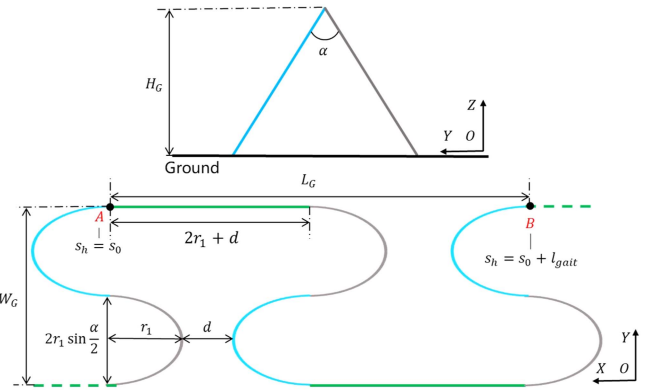


Fig. 15. Projections of gait curve on YOZ and XOY planes, where every other connecting point of cyan and gray parts are contacting the ground.

Fig. 15 plots the projections of crawler gait's target curve on YOZ and XOY planes. Its minimum gait unit comprises six parts, including two straight lines and four half circles. The straight lines are fully in contact with the ground, with Fig. 15 and Table III, the curve's parameters are obtained as

$$\begin{cases} L_G = 4r_1 + 2d \\ W_G = 4r_1 \sin \frac{\alpha}{2} \\ H_G = 2r_1 \cos \frac{\alpha}{2} \\ l_{\text{gait}} = 4(\pi + 1)r_1 + 2d. \end{cases} \quad (23)$$

TABLE IV
ROBOT'S PARAMETERS

Number of joints n	16
Link length l [mm]	95
Link radius r_l [mm]	80
Link mass [g]	about 350
Max joint torque [N·m]	9.9

Modeling crawler gait with (8), (12), and (16) is simpler than that for sidewinding gait since its moving direction is similar to S-pedal gait. Because the straight line part contacts the ground and is located on both sides, considering the nonslip assumption, the direction of d_{curve} is obviously along X -direction with shift control. Therefore, ϕ in (16) is 0, and (8) can be broken up into X - and Y -axes separately as

$$\begin{cases} d_{\text{robot}}^x = d_{\text{curve}}^x - d_{\text{shift}}^x \\ d_{\text{robot}}^y = d_{\text{curve}}^y - d_{\text{shift}}^y = -d_{\text{shift}}^y \end{cases} \quad (24)$$

Substituting (12) into (24), the motion model of the crawler gait with shift control input Δs_h is built as

$$\begin{cases} d_{\text{robot}}^x = \Delta s_h - \frac{\int_{s_h0}^{s_h0+\Delta s_h} ds \cdot e_x}{|e_x|} \\ d_{\text{robot}}^y = -\frac{\int_{s_h0}^{s_h0+\Delta s_h} ds \cdot e_y}{|e_y|} \end{cases} \quad (25)$$

Noticing that the final model for the crawler gait is almost the same as that of the S-pedal one, mainly due to their similarity in the distribution of the ground-contacting parts.

As similarly done for sidewinding gait, the periodic model based on (25) is also presented here. The curve length between point A and point B in Fig. 15 is l_{gait} , which is calculated in (23). When the control input Δs_h is set to l_{gait} , the corresponding \hat{d}_{shift} and \hat{d}_{curve} can be obtained in Fig. 15 as

$$\begin{cases} \hat{d}_{\text{curve}}^x = l_{\text{gait}} = 4(\pi + 1)r_1 + 2d \\ \hat{d}_{\text{shift}}^x = L_G = 4r_1 + 2d \\ \hat{d}_{\text{shift}}^y = 0. \end{cases} \quad (26)$$

Substituting (26) into (24), the periodic motion model for the crawler gait is finally obtained

$$\begin{cases} \hat{d}_{\text{robot}}^x = 4\pi r_1 \\ \hat{d}_{\text{robot}}^y = 0. \end{cases} \quad (27)$$

Also, the crawler model will be verified with the experiment in Section V.

V. EXPERIMENTS AND VALIDATIONS

Based on the models built above, experiments are conducted to verify the proposed modeling approach. The self-built snake robot shown in the center of Fig. 16 is utilized as the testbed, which consists of alternatively connected pitch-axis joints and yaw-axis joints. Specifically, the snake robot has 16 joints with a motion range from -90° to 90° , and other parameters of the robot are provided in Table IV. The link is 95 mm long and wrapped with a rubber ring to ensure enough friction. Although the number of motors is not theoretically required for forming different curves. In experiments, the number of motors(links) is guaranteed to form more than one gait unit for more contacting

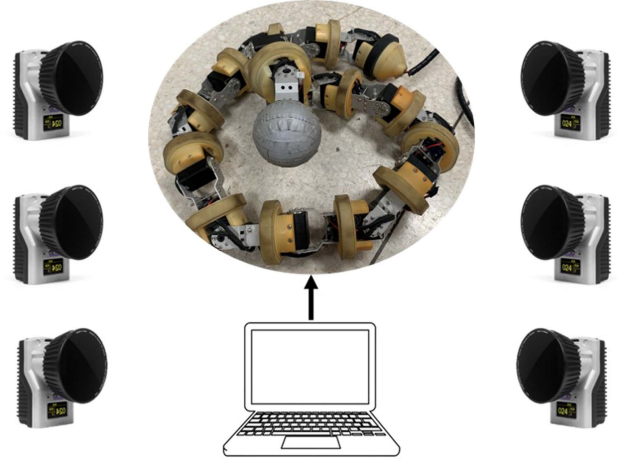


Fig. 16. Experiments are conducted with motion captures to collect the trajectory of the head link of the snake robot, a self-built snake robot with a marker on its head is controlled by a computer to perform different gaits.

points to generate stable movements. Moreover, the motor used has a suitable weight and provides enough torque to execute the calculated joint angles. Each link contains a DYNAMIXEL XH540-W270-R(ROBOTIS) as the actuator which works at the voltage of 12.0 V with a maximum torque of about 9.9 N·m and approximately weighs 350 g.

The snake robot is powered via a cable and the target angle for each joint is sent from a computer through a USB to RS485 conversion. To validate the built models, a marker is attached to the head link of the snake robot. Then a motion capture system (qualisys) is utilized to collect the trajectory of the head link. Three experiments, corresponding to the models built for s-pedal, sidewinding, and crawler gaits, respectively, are conducted to test the performance of the proposed modeling approach.

A. Experiments I: S-Pedal Gait

In the first experiment, the S-pedal gait is designed with parameters: $r_1 = 0.2$ m, $r_2 = 0.15$ m, which are suitable for performing stable movements on the ground. With (6) and (7), β is calculated to be 0.927 rad while $l_{\text{gait}} = 1.64$ m. The periodic motion model of S-pedal gait (15) indicates that when the control input Δs_h increases by l_{gait} , the expected displacement of the snake robot should be \hat{d}_{robot}^x in the X -direction, which is calculated to be 0.84 m, and 0 in the Y -direction. During the experiment, the control input s_h for the snake robot in S-pedal gait is increased from 0 to $3 * l_{\text{gait}} = 4.92$ m, which is expected to move 2.52 m in the X -direction. The collected experimental results are shown in Figs. 17–19, as well as the Supplementary Material, where Fig. 17 shows the moving process of the S-pedal gait, and Fig. 18 provides the trajectories of the head link. The predicted trajectory based on the model is drawn in red, while the blue scatters are the measured one. The missing points on the measured trajectory are caused by the failure of the motion capture system, due to the occasional occlusion of the marker by the robot's body. Despite this, it is clear that the trajectory



Fig. 17. Combination of snake robot performing S-pedal gait.

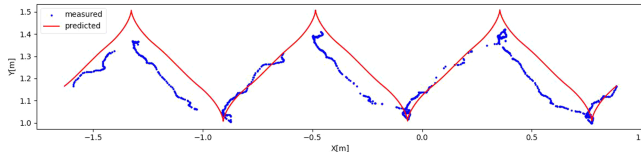


Fig. 18. Plot of trajectories of the head link on the XOY -plane while performing S-pedal gait, the predicted trajectory calculated from the model is drawn in red, while the blue scatters are the measured trajectory. The missing points on the measured trajectory are caused by capturing failure of the motion capture system.

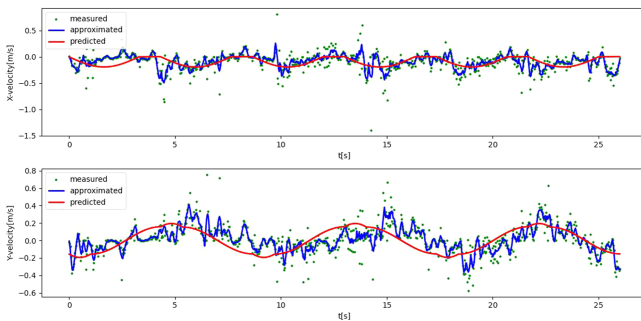


Fig. 19. Plots of velocities of the head link in the X/Y -direction of S-pedal gait, where green dots indicate the measured velocity collected in the experiment, and the predicted velocity is drawn in the red line. The measured velocity is approximated in blue lines with a Savitky–Golay filter.

of the head link is periodic and consists of three cycles, which coincides well with the shift control input $\Delta s_h = 3 * l_{\text{gait}}$. The measured magnitude of displacement in the X -direction is 2.47 m, with a 1.9% error from the expected 2.52 m. In the directional respect, the measured direction of displacement is 2.2° , while the predicted direction is 0° , which means along the X -axis. Mainly, the error is caused by the approximation in gait generation, which uses the snake robot with a discrete structure to approximate the target shape curve designed by the backbone curve method.

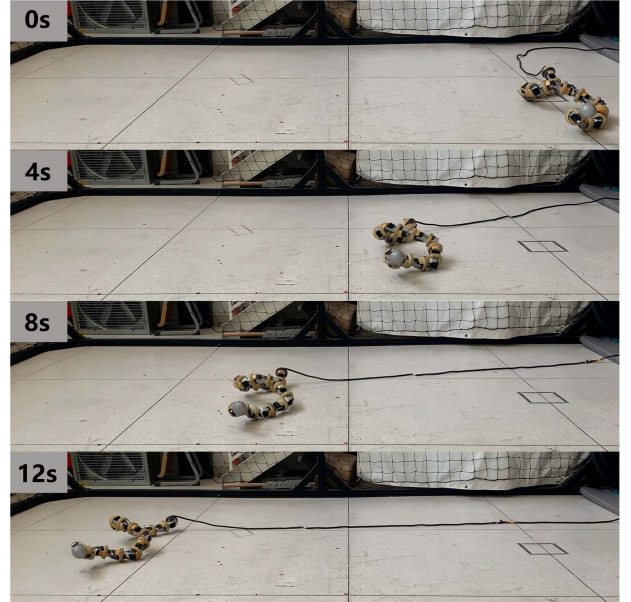


Fig. 20. Combination of snake robot performing sidewinding gait.

Fig. 19 plots the velocities of the head link in the X/Y -direction of S-pedal gait, where the green dots indicate the measured velocity collected in the experiment, and the predicted velocity is drawn in the red line. They are calculated based on the predicted and measured trajectories shown in Fig. 18. Because of some missing points caused by occlusions of the marker, the measured velocities are discrete and hard to analyze, and also they are contaminated by measuring noise. To provide a clear comparison with predicted velocities, the measured velocity is approximated in blue lines with a Savitzky–Golay filter whose window length and order are 9 and 2, respectively. Despite some deviations caused by measuring noise and gait generation approximation, the approximated velocities are sufficiently close to the predicted ones in both directions.

B. Experiments II: Sidewinding Gait

To validate the generality of the proposed modeling approach, a sidewinding gait with parameter $r_1 = 0.15$ m is constructed and then applied to the snake robot. Based on (17) and (18), l_{gait} and ϕ is calculated to be 0.94 m and 0.31 rad, respectively.

The periodic motion model of sidewinding gait (22) indicates that when the control input Δs_h increases by l_{gait} , the expected displacement of snake robot should be \hat{d}_{robot}^x in the X -direction and \hat{d}_{robot}^y in the Y -direction, which, respectively, are calculated to be 0.88 m and 0.27 m. During the experiment, the control input s_h for the snake robot in sidewinding gait is increased from 0 to $3 * l_{\text{gait}} = 2.82$ m, which is expected to move 2.64 m in the X -direction, 0.81 m in the Y -direction. The collected experimental results are shown in Figs. 20–22, as well as the Supplementary Material, where Fig. 20 shows the moving process of the sidewinding gait, and Fig. 21 provides the trajectories of the head link. The predicted trajectory based on (20) is drawn in red, while the blue scatters are the measured trajectory. Obviously, the trajectory of the head link is

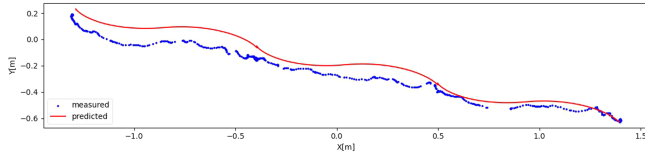


Fig. 21. Plots of trajectories of head link while performing sidewinding gait. The predicted trajectory is drawn in red, while the blue scatters are the measured trajectory with some missing points caused by the capturing failure.

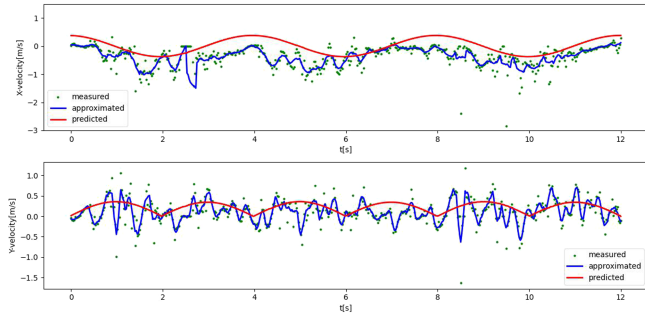


Fig. 22. Plots of velocities of the head link in the X/Y -direction of sidewinding gait, where green dots indicate the measured velocity collected in the experiment, and the predicted velocity is drawn in the red line. The measured velocities are approximated in blue lines with a Savitzky–Golay filter.

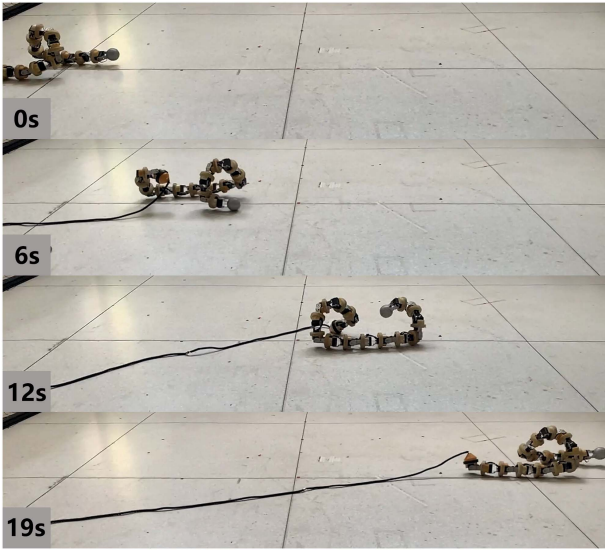


Fig. 23. Combination of snake robot performing crawler gait.

also periodic with three cycles which coincides well with the shift control input. The measured magnitude displacements are, respectively, 2.69 m in the X -direction, with a 1.8% error from the expected 2.64 m, and 0.79 m in the Y -direction, with a 2.4% error from the expected 0.81 m. In the directional respect, the measured direction of displacement is 16.4° , with a 3.5% error from the expected 17.0° . Please note that this is the direction of sidewinding motion d_{robot} , not the direction angle ϕ of d_{curve} .

Fig. 22 plots the velocities of the head link in the X/Y -direction of sidewinding gait, where the green dots indicate the measured velocity collected in the experiment, and the predicted velocity

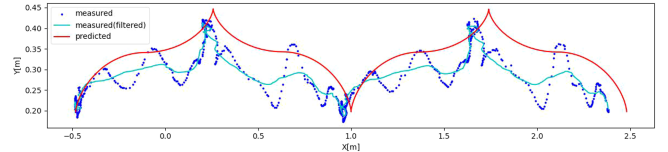


Fig. 24. Plots of trajectories of head link while performing crawler gait. The predicted trajectory is drawn with the red line, while the scatters are the measured ones. The oscillations in the Y -direction are caused by the swaying of crawler gait as shown in the supplemental video, it is filtered as the cyan line.

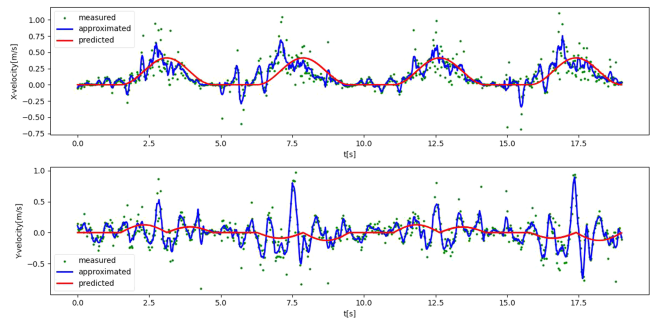


Fig. 25. Plots of velocities of the head link in the X/Y -direction of crawler gait, where green dots indicate the measured velocity collected in the experiment, and the predicted velocity is drawn in the red line. The measured velocities are approximated in blue lines with a Savitzky–Golay filter.

is drawn in the red line. They are both calculated based on the predicted and measured trajectories shown in Fig. 21. To provide a clear comparison with the predicted velocities, the measured velocity is approximated in blue lines with a Savitzky–Golay filter whose window length and order are 9 and 2, respectively. Despite some deviations caused by gait generation approximation and measuring noise, the approximated velocities are sufficiently close to the predicted ones in both directions.

C. Experiments III: Crawler Gait

In the third experiment, the snake robot performs a crawler gait with parameters $r_1 = 0.117$ m, $d = 0.12$ m, and $\alpha = 1.11$ rad. Based on (23), l_{gait} is calculated to be 2.19 m. The periodic motion model of S-pedal gait (27) indicates that when the control input Δs_h increases by l_{gait} , the expected displacement of the snake robot should be \dot{d}_{robot}^x in the X -direction, which is calculated to be 1.98 m and 0 in Y -direction. During the experiment, the control input s_h for the snake robot in S-pedal gait is increased from 0 to $2 * l_{\text{gait}} = 4.38$ m, which is expected to move 2.96 m in the X -direction. The collected experimental results are shown in Figs. 23–25, as well as the Supplementary Material, where Fig. 23 shows the moving process of the crawler gait, and Fig. 24 provides the trajectory of the head link. Also, the predicted trajectory is drawn with a red line while scatters are the measured one. The oscillations of the experimental results in the Y -direction within the gait's width of 0.25 m are caused by the swaying of the crawler gait as shown in the supplemental video. The measured displacement is filtered and drawn in the cyan line, details of the filter are provided in the following remark. Despite the swaying, it is clear that the trajectory of the head link

TABLE V
ACCURACY COMPARISON WITH EXISTING METHODS

	magnitude of displacement d (meters)			direction of displacement ϕ (degree)		
	predicted	measured	error percentage	predicted	measured	error percentage
Transeth et al. [33] sidewinding	1.2m	1.01m	15.8%	not available	8.5°	N/A
Enner et al. [34] sidewinding	not available	not available	5%	not available	11°	N/A
ours(below) sidewinding	2.76m	2.80m	1.4%	17.0°	16.4°	3.5%
S-pedal	2.52m	2.47m	1.9%	0°	2.2°	N/A
crawler	2.96m	2.86m	3.3%	0°	1.7°	N/A

is periodic and consists of two cycles, which coincides well with the shift control input. The measured magnitude of displacement in the X -direction is 2.86 m, with a 3.3% error from the expected 2.96 m. In the directional respect, the measured direction of displacement is 1.7°, while the predicted direction is 0°, which means along the X -axis. The error is relatively larger than the other two gaits, mainly because crawler gaits involve a smaller arc radius, which leads to greater joint angles, possibly near ±90° during the motion. As a result, larger joint angles further amplify the approximating error of the gait generation method. Noting that as the snake robot's length is limited, it is difficult to further enlarge the arc radius on this testbed while guaranteeing stable movements simultaneously.

Fig. 25 plots the velocities of the head link in the X/Y -direction of crawler gait, where the green dots indicate the measured velocity collected in the experiment, and the predicted velocity is drawn in the red line. They are both calculated based on the predicted and measured trajectories shown in Fig. 24. To provide a clear comparison with the predicted velocities, the measured velocity is approximated in blue lines with a Savitzky–Golay filter whose window length and order are 9 and 2, respectively. Despite some deviations caused by gait generation approximation and measuring noise, the approximated velocities are sufficiently close to the predicted ones in the X -direction. But unlike the other two gaits, because of the swaying of the crawler gait mentioned before, there are oscillations in the Y -direction.

Remark: Since the swaying is caused by the length limitation of the snake robot, it should not be considered a modeling error. Therefore, a Savitzky–Golay filter is applied and the filtered trajectory is drawn in cyan to evaluate our modeling approach better. To eliminate the oscillation in the Y -direction, the window length and order of the polynomial of the filter are set to 29 and 1, respectively.

D. Comparison With Existing Results

To demonstrate the advantage of the proposed method, a thorough comparison based on experimental results and existing results is made. Considering that it is not suitable to compare with those data-diving or control-to-action mapping methods, the comparison is made with earlier results which model the motion directly and provide experimental results [33], [34]. These two articles verify their methods on sidewinding gait and other gaits such as rolling, slithering, and so on. The

sidewinding motion is chosen for comparison since it is modeled in all three works. Please note that although [35] also presents a motion modeling of sidewinding gaits, its motion modeling predicts the average velocity with a percentage of errors less than 6.1%, the accumulated errors of displacements in direction and magnitude are not provided. Therefore, it is not listed and compared in Table V. As shown in Table V, despite that some of the experimental results are not available in those articles, our method achieves the most precise predictions in both the magnitude and direction of the displacement. For comparison methods, the percentage error on the magnitude of displacement of sidewinding is 15.8% and 5%, respectively. While the proposed method yields a percentage error of 1.4% with an even longer moving distance. Moreover, the proposed modeling approach successfully models the direction of motion based on the target curve, while the comparative ones cannot predict the direction at all. The experiments show satisfactory results on direction prediction, with a 3.5% error of sidewinding gait. For the other two commonly used gait generated by the backbone curve method, the proposed motion modeling method yields supreme accurate results as well, with the magnitude error percentage always less than 3.3%. Please note that, unlike the sidewinding gait, the predicted direction angle of these two gaits equals 0. Therefore, the percentage error is meaningless here, and experimental results prove that the direction error is always less than 3°.

VI. CONCLUSION

This article studied the problem of modeling 3-D snake robot motion on the ground, and it proposed a unified motion modeling approach for gaits generated by the backbone curve method.

Specifically, a novel recognition was proposed, which considered the target backbone curve as a real entity with the ability to move. By utilizing this recognition, the movement of the snake robot can be decomposed into two parts, namely, the movement of the target backbone curve and the movements of the snake robot along the backbone bone curve. These two movements were explicitly related to the backbone curve's parameters and control's input. Then, considering the actual movement of a snake robot, a nonslip assumption was made, based on which, the ground-contacting statements of the snake robot's links during shift control were carefully analyzed, to determine the moving direction of the target backbone curve. Finally, the motion model was built with the two movements obtained. Based on

the proposed approach, three widely used gaits generated by the backbone curve method were successfully modeled. Three groups of experiments were conducted to verify the obtained model of these gaits. As indicated by the collected results, the constructed models were highly accurate with errors always less than 3.5%, indicating the effectiveness of the proposed modeling approach. Compared with the existing method, the proposed modeling approach achieved a much more precise prediction, both in the direction and magnitude of motions.

Future work targets extending the proposed modeling approach to wider situations, as well as considering improvements to further increase the modeling accuracy of the proposed modeling approach.

REFERENCES

- [1] J. Whitman, N. Zevallos, M. Travers, and H. Choset, "Snake robot urban search after the 2017 Mexico city earthquake," in *Proc. IEEE Int. Symp. Saf. Secur. Rescue Robot.*, 2018, pp. 1–6.
- [2] D. Li, Z. Pan, H. Deng, and L. Hu, "Adaptive path following controller of a multijoint snake robot based on the improved serpenoid curve," *IEEE Trans. Ind. Electron.*, vol. 69, no. 4, pp. 3831–3842, Apr. 2022.
- [3] Z. Cao, D. Zhang, and M. Zhou, "Modeling and control of hybrid 3-D gaits of snake-like robots," *IEEE Trans. Neural Netw. Learn. Syst.*, vol. 32, no. 10, pp. 4603–4612, Oct. 2021.
- [4] Z. Cao, D. Zhang, and M. Zhou, "Direction control and adaptive path following of 3-D snake-like robot motion," *IEEE Trans. Cybern.*, vol. 52, no. 10, pp. 10980–10987, Oct. 2022.
- [5] L. Liu, W. Xi, X. Guo, and Y. Fang, "Vision-based path following of snake-like robots," in *Proc. IEEE Int. Conf. Robot. Autom.*, 2021, pp. 3084–3090.
- [6] L. Liu, X. Guo, and Y. Fang, "A reinforcement learning-based strategy of path following for snake robots with an onboard camera," *Sensors*, vol. 22, no. 24, 2022, Art. no. 9867. [Online]. Available: <https://www.mdpi.com/1424-8220/22/24/9867>
- [7] J. W. Burdick, J. Radford, and G. S. Chirikjian, "A 'sidewinding' locomotion gait for hyper-redundant robots," *Adv. Robot.*, vol. 9, no. 3, pp. 195–216, 1994.
- [8] C. Gong, R. L. Hatton, and H. Choset, "Conical sidewinding," in *Proc. IEEE Int. Conf. Robot. Autom.*, 2012, pp. 4222–4227.
- [9] R. L. Hatton and H. Choset, "Sidewinding on slopes," in *Proc. IEEE Int. Conf. Robot. Autom.*, 2010, pp. 691–696.
- [10] B. Chong et al., "Frequency modulation of body waves to improve performance of sidewinding robots," *Int. J. Robot. Res.*, vol. 40, no. 12/14, pp. 1547–1562, 2021.
- [11] B. Chong et al., "A hierarchical geometric framework to design locomotive gaits for highly articulated robots," in *Robotics: Sci. Syst.*, 2019.
- [12] B. Chong et al., "Coordination of back bending and leg movements for quadrupedal locomotion," in *Robotics: Sci. Syst.*, vol. 20, 2018.
- [13] C. Gong, Z. Ren, J. Whitman, J. Grover, B. Chong, and H. Choset, "Geometric motion planning for systems with toroidal and cylindrical shape spaces," in *Proc. Dynamic Syst. Control Conf.*, 2018, Art. no. V003T32A013.
- [14] D. Rollinson and H. Choset, "Gait-based compliant control for snake robots," in *Proc. IEEE Int. Conf. Robot. Autom.*, 2013, pp. 5138–5143.
- [15] T. Takemori, M. Tanaka, and F. Matsuno, "Adaptive helical rolling of a snake robot to a straight pipe with irregular cross-sectional shape," *IEEE Trans. Robot.*, vol. 39, no. 1, pp. 437–451, Feb. 2023.
- [16] W. Huang, X. Guo, H. Liu, and Y. Fang, "A robust model-based radius estimation approach for helical climbing motion of snake robots," *IEEE/ASME Trans. Mechatron.*, vol. 28, no. 6, pp. 3284–3293, Dec. 2023.
- [17] B. A. Elsayed, T. Takemori, M. Tanaka, and F. Matsuno, "Mobile manipulation using a snake robot in a helical gait," *IEEE/ASME Trans. Mechatron.*, vol. 27, no. 5, pp. 2600–2611, Oct. 2022.
- [18] R. Wang, W. Xi, X. Guo, and Y. Fang, "Path following for snake robot using crawler gait based on path integral reinforcement learning," in *Proc. 6th IEEE Int. Conf. Adv. Robot. Mechatron.*, 2021, pp. 192–198.
- [19] M. Tesch et al., "Parameterized and scripted gaits for modular snake robots," *Adv. Robot.*, vol. 23, no. 9, pp. 1131–1158, 2009.
- [20] D. Rollinson and H. Choset, "Pipe network locomotion with a snake robot," *J. Field Robot.*, vol. 33, no. 3, pp. 322–336, 2016.
- [21] H. Yamada and S. Hirose, "Study on the 3 D shape of active cord mechanism," in *Proc. IEEE Int. Conf. Robot. Autom.*, 2006, pp. 2890–2895.
- [22] S. B. Andersson, "Discretization of a continuous curve," *IEEE Trans. Robot.*, vol. 24, no. 2, pp. 456–461, Apr. 2008.
- [23] H. Yamada, S. Takaoka, and S. Hirose, "A snake-like robot for real-world inspection applications (the design and control of a practical active cord mechanism)," *Adv. Robot.*, vol. 27, no. 1, pp. 47–60, 2013.
- [24] T. Takemori, M. Tanaka, and F. Matsuno, "Gait design for a snake robot by connecting curve segments and experimental demonstration," *IEEE Trans. Robot.*, vol. 34, no. 5, pp. 1384–1391, Oct. 2018.
- [25] T. Wang et al., "Reconstruction of backbone curves for snake robots," *IEEE Robot. Autom. Lett.*, vol. 6, no. 2, pp. 3264–3270, Apr. 2021.
- [26] T. Takemori, M. Tanaka, and F. Matsuno, "Ladder climbing with a snake robot," in *Proc. IEEE/RSJ Int. Conf. Intell. Robots Syst.*, 2018, pp. 1–9.
- [27] T. Takemori, M. Tanaka, and F. Matsuno, "Hoop-passing motion for a snake robot to realize motion transition across different environments," *IEEE Trans. Robot.*, vol. 37, no. 5, pp. 1696–1711, Oct. 2021.
- [28] M. Inazawa, T. Takemori, M. Tanaka, and F. Matsuno, "Motion design for a snake robot negotiating complicated pipe structures of a constant diameter," in *Proc. IEEE Int. Conf. Robot. Autom.*, 2020, pp. 8073–8079.
- [29] M. Inazawa, T. Takemori, M. Tanaka, and F. Matsuno, "Unified approach to the motion design for a snake robot negotiating complicated pipe structures," *Front. Robot. AI*, vol. 8, 2021, Art. no. 629368.
- [30] R. L. Hatton and H. Choset, "Generating gaits for snake robots: Annealed chain fitting and keyframe wave extraction," *Auton. Robots*, vol. 28, pp. 271–281, 2010.
- [31] Z. Ji, G. Song, F. Wang, Y. Li, and A. Song, "Design and control of a snake robot with a gripper for inspection and maintenance in narrow spaces," *IEEE Robot. Autom. Lett.*, vol. 8, no. 5, pp. 3086–3093, May 2023.
- [32] Z. Bing, L. Cheng, G. Chen, F. Röhrbein, K. Huang, and A. Knoll, "Towards autonomous locomotion: CPG-based control of smooth 3D slithering gait transition of a snake-like robot," *Bioinspiration Biomimetics*, vol. 12, no. 3, 2017, Art. no. 035001.
- [33] A. A. Transeth, R. I. Leine, C. Glocker, and K. Y. Pettersen, "3-D snake robot motion: Nonsmooth modeling, simulations, and experiments," *IEEE Trans. Robot.*, vol. 24, no. 2, pp. 361–376, Apr. 2008.
- [34] F. Enner, D. Rollinson, and H. Choset, "Simplified motion modeling for snake robots," in *Proc. IEEE Int. Conf. Robot. Autom.*, 2012, pp. 4216–4221.
- [35] K. Melo, "Modular snake robot velocity for side-winding gaits," in *Proc. IEEE Int. Conf. Robot. Autom.*, 2015, pp. 3716–3722.
- [36] Y. Hwang and M. Ishikawa, "Generative locomotion model of snake robot with hierarchical networks for topological representation," in *Proc. Int. Conf. Agents Artif. Intell.*, 2020, pp. 194–202.
- [37] R. Wang, W. Xi, X. Guo, and Y. Fang, "Path following for snake robot using crawler gait based on path integral reinforcement learning," in *Proc. IEEE 6th Int. Conf. Adv. Robot. Mechatron.*, 2021, pp. 192–198.
- [38] A. H. Chang and P. A. Vela, "Shape-centric modeling for control of traveling wave rectilinear locomotion on snake-like robots," *Robot. Auton. Syst.*, vol. 124, 2020, Art. no. 103406.
- [39] W. Zhen, C. Gong, and H. Choset, "Modeling rolling gaits of a snake robot," in *Proc. IEEE Int. Conf. Robot. Autom.*, 2015, pp. 3741–3746.
- [40] H. Yamada and S. Hirose, "Study of active cord mechanism," *J. Robot. Soc. Jpn.*, vol. 26, no. 1, pp. 110–120, 2008.
- [41] H. Marvi et al., "Sidewinding with minimal slip: Snake and robot ascent of sandy slopes," *Science*, vol. 346, no. 6206, pp. 224–229, 2014.



Wei Huang received the B.S. degree in intelligent science and technology from Nankai University, Tianjin, China, in 2020, where he is currently working toward the Ph.D. degree in control science and engineering, with the Institute of Robotics and Automatic Information Systems.

His current research interests include control of biologically inspired robots and reinforcement learning.



Yongchun Fang (Senior Member, IEEE) received the B.S. and M.S. degrees in control theory and applications from Zhejiang University, Hangzhou, China, in 1996 and 1999, respectively, and the Ph.D. degree in electrical engineering from Clemson University, Clemson, SC, USA, in 2002.

From 2002 to 2003, he was a Postdoctoral Fellow with the Sibley School of Mechanical and Aerospace Engineering, Cornell University, Ithaca, NY, USA. He is currently a Professor with the Institute of Robotics and Automatic Information Systems, Nankai University, Tianjin, China. His current research interests include nonlinear control, visual servoing, control of underactuated systems, and AFM-based nanosystems.



Xian Guo (Member, IEEE) received the B.S. degree in mechanical design, manufacturing, and automation from the Huazhong University of Science and Technology, Wuhan, China, in 2009, and the Ph.D. degree in mechatronics from the Shenyang Institute of Automation, Chinese Academy of Sciences, Shenyang, China, in 2016.

From 2016 to 2018, he was a Postdoctoral Fellow with Nankai University, Tianjin, China, where he is currently an Associate Professor with the Institute of Robotics and Automatic Information Systems. His current research interests include modeling and control of biorobots and reinforcement learning.



Huawang Liu received the B.S. degree in intelligence science and technology from the Hebei University of Technology, Tianjin, China, in 2014, and the M.S. degree in electronic engineering from the University of Melbourne, Melbourne, Australia, in 2017.

After that, he worked as an Experimenter with Nankai University. His research interests include robotics and electronic design and applications.



Lixing Liu received the B.S. degree in intelligent science and technology from the Hebei University of Technology, Tianjin, China, in 2020, where she is currently working toward the Ph.D. degree in control science and engineering with the Institute of Robotics and Automatic Information Systems.

Her current research interests include control of biologically inspired robots and reinforcement learning.